arXiv:cond-mat/0502341v2 [cond-mat.supr-con] 8 Jan 2006

Superconductivity induced by spark erosion in $ZrZn_2$

E. A. Yelland, S. M. Hayden, and S. J. C. Yates
H. H. Wills Physics Laboratory, University of Bristol, Tyndall Avenue, Bristol BS8 1TL, United Kingdom

C. Pfleiderer,* M. Uhlarz, R. Vollmer, and H. v. Löhneysen
Physikalishes Institut, Universitat Karlsruhe, D-76128 Karlsruhe, Germany

N. R. Bernhoeft
DRFMC-SPSMS, CEA Grenoble, F-38054 Grenoble, Cedex 9, France

R. P. Smith and S. S. Saxena
Cavendish Laboratory, University of Cambridge, Madingley Road, Cambridge CB3 0HE, United Kingdom

N. Kimura
Center for Low Temperature Science, Tohoku University, Sendai, Miyagi 980-8578, Japan
(Dated: March 23, 2022)

We show that the superconductivity observed recently in the weak itinerant ferromagnet $ZrZn_2$ [C. Pfleiderer *et al.*, Nature (London) **412**, 58 (2001)] is due to remnants of a superconducting layer induced by spark erosion. Results of resistivity, susceptibility, specific heat and surface analysis measurements on high-quality $ZrZn_2$ crystals show that cutting by spark erosion leaves a superconducting surface layer. The resistive superconducting transition is destroyed by chemically etching a layer of $5\,\mu$m from the sample. No signature of superconductivity is observed in $\rho(T)$ of etched samples at the lowest current density measured, $J = 675\,\mathrm{Am}^{-2}$, and at $T \geq 45\,$mK. EDX analysis shows that spark-eroded surfaces are strongly Zn depleted. The simplest explanation of our results is that the superconductivity results from an alloy with higher Zr content than $ZrZn_2$.

PACS numbers: 75.50.Cc, 74.70.Ad, 74.25.Fy, 74.70.-b

I. INTRODUCTION

Ferromagnetism in the cubic Laves compound $ZrZn_2$ was first discovered by Matthias and Bozorth[1] in 1958. Since this time, $ZrZn_2$ has attracted considerable theoretical and experimental attention. In particular, some authors have suggested that metals which are close to a ferromagnetic instability at low temperatures, such as $ZrZn_2$, may exhibit magnetically mediated p-wave superconductivity[2,3]. In principle, $ZrZn_2$ is an ideal material in which to search for such p-wave superconductivity because it can be driven into the paramagnetic state by application of relatively modest pressures[4]. However, until recently, experiments failed to find any evidence for superconductivity in $ZrZn_2$ [5,6,7,8].

Signatures of weak superconductivity were recently reported in the magnetic and transport properties of $ZrZn_2$ [9]. In this paper, we show that spark erosion, a standard procedure for cutting metallic samples, can produce a superconducting surface layer on $ZrZn_2$ at ambient pressure. The samples used in the present work are from the same ingot as those used in Ref. 9 and have residual resistance ratios (RRR's) as high as 105.

II. EXPERIMENTAL DETAILS

$ZrZn_2$ melts congruently at 1180°C[10,11]. At this temperature zinc has a vapor pressure of about 10 bars and is an aggressive flux. Thus we chose to grow $ZrZn_2$ by a directional cooling technique[12]. Stoichiometric quantities of high-purity zone-refined Zr (99.99%, Materials Research MARZ grade) and Zinc (99.9999%, Metal Crystals) were loaded into a Y_2O_3 crucible. The total charge used was 4.2 g. The crucible was sealed inside a tantalum bomb which was closed by electron beam welding under vacuum. The assembly was heated to 1210°C and then cooled through the melting point at $2^\circ\mathrm{C\,hr}^{-1}$. The ingot was then annealed by cooling to 500°C over a period of 72 hr. This method produced single crystals of volumes up to approximately 0.4 cm^3. Single crystals produced in this way had residual resistivities as low as $\rho_0 = 0.53\,\mu\Omega$cm corresponding to RRR = $\rho(293K)/\rho(T \to 0) = 105$. This corresponds to a quasiparticle mean free path $\ell = 1500\,$Å (assuming a Fermi surface area $S_F = 1.9 \times 10^{21}$ m^{-2} , as given by bandstructure calculations[13]).

All experiments reported here were measured at ambient pressure. Resistivity measurements were made using a standard a.c. technique using a Brookdeal 9433 lownoise transformer and SR850 digital lock-in amplifier. Most measurements were made at a frequency f=2 Hz. Sample contacts were made with Dupont 4929 Ag/epoxy.

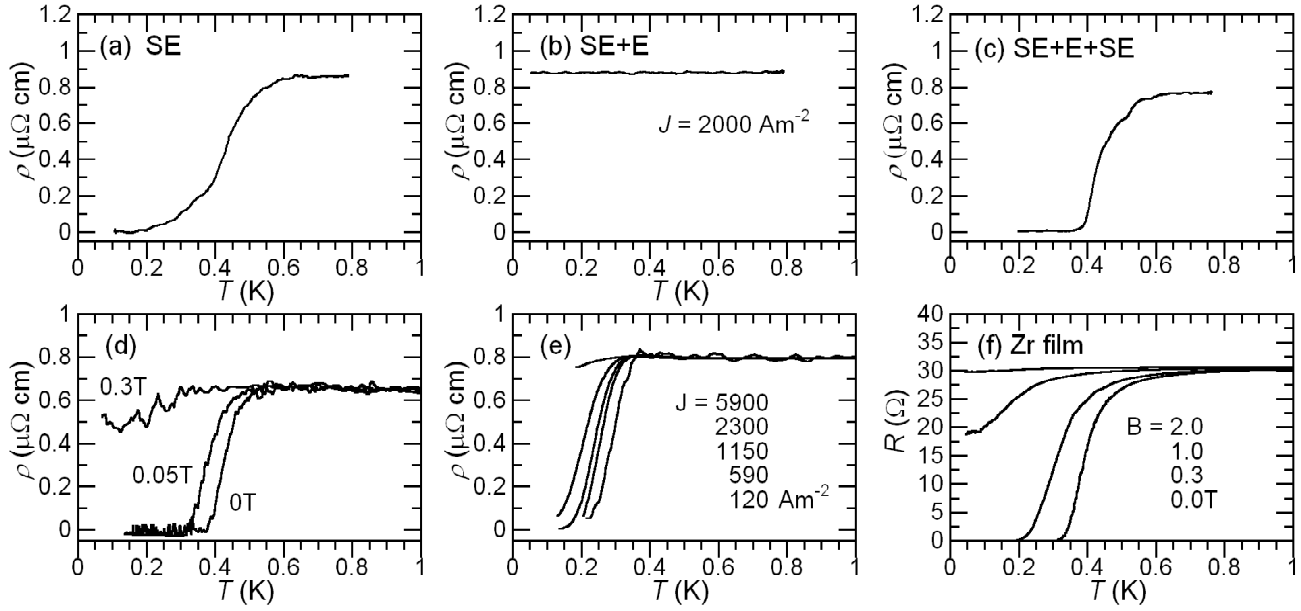


FIG. 1: (a)-(e) The temperature dependence of the resistivity of $ZrZn_2$ under various conditions and for different sample treatments. The current density J is calculated using the bulk cross-sectional area of the sample. (a) As grown sample cut by spark erosion ($B = 0\,\mathrm{T}$, $J = 2000\,\mathrm{Am}^{-2}$); (b) as (a) followed by HF/HNO_3 etching ($B = 0\,\mathrm{T}$, $J = 2000\,\mathrm{Am}^{-2}$); (c) as (b) followed by further spark erosion ($B = 0\,\mathrm{T}$, $J = 2000\,\mathrm{Am}^{-2}$); (d) The effect of applied field on $\rho(T)$ of a spark-eroded sample. (e) The dependence on current density of $\rho(T)$ of a spark-eroded sample. (f) $\rho(T, B)$ for a zirconium film with a magnetic field applied in plane of film.

Heat capacity measurements were made using a long-pulse technique in which the sample was mounted on a silicon platform connected to a temperature-controlled stage by a thin copper wire.

Energy dispersive X-ray (EDX) analysis of sample surfaces was performed on a Jeol JSM-5600LV scanning electron microscope using a 20 kV incident electron beam. In order to make quantitative composition estimates, we recorded EDX spectra from sample surfaces and from elemental standards under identical conditions. All surfaces analyzed, except the spark-eroded surface, were prepared by polishing with 0.1 μm diamond lapping film in order to minimize errors due to geometrical effects.

III. RESULTS

A. Resistivity

Fig. 1 shows the temperature dependence of the resistivity for $ZrZn_2$ under various conditions and for different sample treatments. In order to make resistivity measurements, bar-shaped samples were cut from the ingot by spark erosion using Mo wire. Fig. 1(a) shows the $\rho(T)$ curve for a sample with all surfaces produced by spark erosion. A superconducting transition is observed with an onset temperature (T_{SC}) of about 0.6 K. To test whether the superconductivity is a bulk property or a property of the spark-eroded surfaces, we then etched the sample used in Fig. 1(a) in a solution containing 12 parts by volume of 69% HNO_3, 5 parts 48% HF and 1000 parts H_2O for 1 minute. This removed 5% of the sample mass, corresponding to a surface layer 5 μm thick. Fig. 1(b) shows the resistivity measured after etching: the superconducting transition has been removed. The sample was then spark-cut along its length to give two pieces, each having one spark-eroded surface. Panel (c) shows $\rho(T)$ for one of these. The superconducting transition has been restored. These results were obtained with the voltage contacts on the spark-eroded surface, but identical behavior was observed when the experiment was repeated on another sample with the same treatment history and voltage contacts were placed on the etched surface opposite to the spark-eroded one. On this occasion, Cu wire was used as the spark-cutter electrode so contamination from the wire is excluded as a cause of surface superconductivity. The disappearance of superconductivity after etching and its subsequent reappearance after spark-cutting was reproduced in another sample. In well etched samples no sign of superconductivity was observed at the lowest current density measured $J = 675\,\mathrm{Am}^{-2}$ and the lowest temperature $T = 45\,\mathrm{mK}$.

We also investigated the magnetic field dependence of the superconducting transition in spark-eroded $ZrZn_2$ samples. Fig. 1(d) shows the resistive transitions measured with a magnetic field applied perpendicular to the current and parallel to one of the spark-eroded surfaces; the superconducting anomaly persists to fields

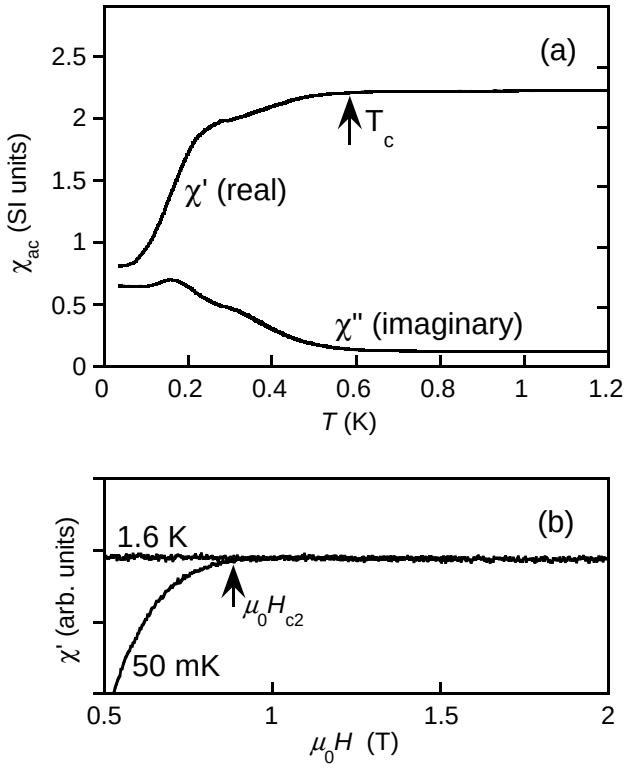


FIG. 2: (a) The temperature dependence of the a.c. susceptibility of $ZrZn_2$ (sample CY). Measurements were made with a modulation field of amplitude $b = 1.2$ μT and frequency f = 1.17 kHz. The large susceptibility in the normal state is due to the presence of ferromagnetism. (b) The field dependence of the a.c. susceptibility measured with the same modulation amplitude and frequency as the main figure.

$\mu_0 H > 0.3$ T. At first glance this implies a surprisingly high critical field to critical temperature ratio but as we discuss later this is easily explained by the reduction of the Meissner screening in a layer that is thin compared to the superconducting penetration depth. Fig. 1(f) shows resistivity results for a Zr film which will be compared with our results on $ZrZn_2$ below. The film was produced by evaporation of Zr wire on to a glass substrate under a vacuum of $\approx 10^{-5}$ torr. The film thickness is estimated as $\sim$ 500 nm. Superconductivity persists with in-plane magnetic fields up to ~ 1 T.

B. Susceptibility

Fig. 2 shows a.c. susceptibility measurements made on a spark-eroded sample of $ZrZn_2$. The susceptometer was calibrated by measuring the superconducting transition of an indium sample at low frequencies (f=1.5–5 Hz). The data have not been corrected for the effects of the demagnetization field. Fig. 2(a) shows that both the real and imaginary components of the susceptibility (χ' and χ'') are large in the temperature range $0.6 < T < 1.2$ K,

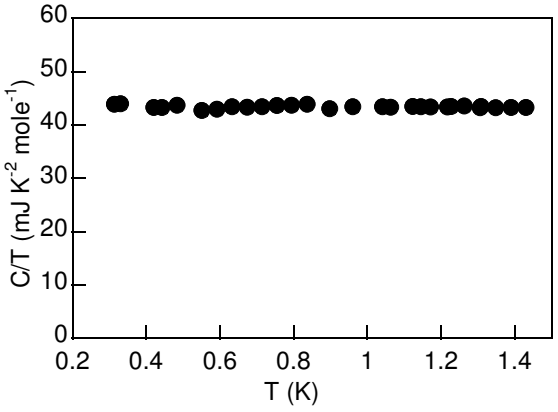


FIG. 3: The specific heat capacity of $ZrZn_2$ (sample CS) in zero applied field measured by a relaxation method. The absence of a heat capacity anomaly at T_{SC} strongly suggests that the bulk is not superconducting above 0.3 K.

due to the alignment of ferromagnetic domains by the applied field. Below the onset temperature of the spark erosion-induced superconductivity $T_{SC} \approx 0.6$ K, the real part of the susceptibility begins to drop and the imaginary part starts to increase. There is a large drop in the susceptibility $\Delta\chi' \approx 2$, however full Meissner screening $[\chi' = -1/(1-N)]$ is not observed. We estimate the demagnetization factor of the sample to be $N \approx 0.2$. It appears that spark erosion induces a thin superconducting layer which partially shields the ferromagnetic core. Fig. 2(b) shows the a.c. susceptibility measured in the presence of d.c. magnetic fields up to 2 T for T=0.05 K and T=1.6 K. The difference between the 0.05 K and 1.6 K curves shows that some parts of the sample have critical fields up to 0.9 T.

C. Heat Capacity

One of the most direct signatures of bulk superconductivity is the specific heat anomaly. Fig. 3 shows the specific heat capacity, plotted as $C(T)/T$, for a sample (CS) cut from a region of the ingot next to that used for the resistivity and susceptibility measurements. As in previous work[9], no specific heat capacity anomaly is observed, strongly suggesting the absence of bulk superconductivity above $T = 0.3$ K in this sample.

D. EDX Analysis

We have demonstrated above that spark erosion of $ZrZn_2$ induces a superconducting layer. In order to determine the nature of the changes in the surface layer that cause the behavior shown in Figs. 1(a-c), we performed spot-mode EDX analysis on a spark-cut surface of a superconducting $ZrZn_2$ sample [Fig. 4(b)] and on a

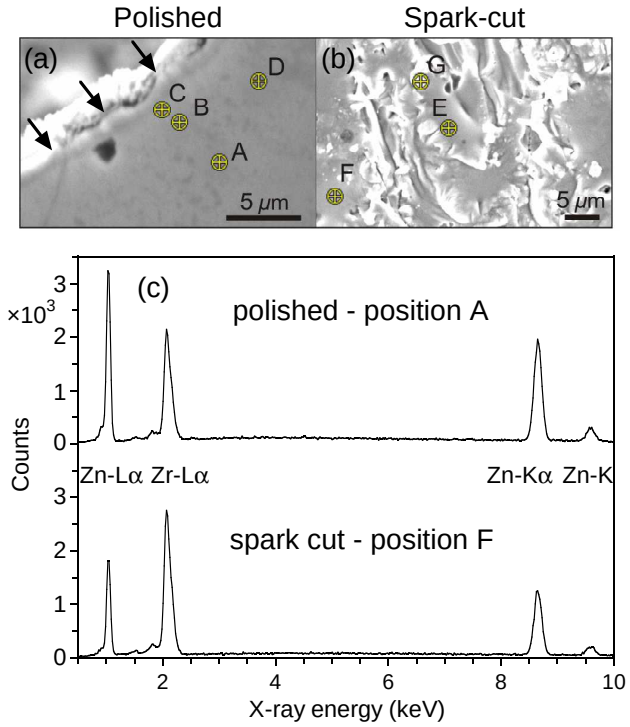


FIG. 4: Panel (a): SEM image of a polished $ZrZn_2$ sample. The polished face is normal to the incident electron beam; the sample edge, indicated by arrows, is defined by a spark-cut surface that is approximately parallel to the beam. Thus the EDX analysis at position C probes a region $1-2\,\mu$m below the spark-cut face. Panel (b): SEM image of a spark-cut sample. Panel (c): examples of raw EDX spectra obtained on spark-cut and polished samples, showing Zn depletion of the spark-cut surface.

peaks analysed	Zr-Lα/Zn-Kα		Zr-Lα/Zn-Lα	
	Zr(%)	Zn(%)	Zr(%)	Zn(%)
Position	polished			
A	31.5	68.5	33.0	67.0
B	31.6	68.4	33.0	67.0
C	32.2	67.8	33.3	66.7
D	31.7	68.3	32.8	67.2
	spark-cut			
E	49.1	50.9	42.2	57.8
F	47.3	52.7	48.8	51.2
G	71.1	28.9	67.7	32.3

TABLE I: Atomic concentration results of spot EDX analysis on polished and spark-cut samples of $ZrZn_2$. The position labels correspond to those in Fig. 4. A ZAF correction procedure using pure element standards was used to calculate atomic concentrations. Two characteristic Zn peaks, Zn-Kα (8.6 keV) and Zn-Lα (1.0 keV), were used to give two distinct concentration estimates; the agreement of the two estimates shows that the roughness of the spark-cut surface does not prevent a quantitative analysis. We conclude that the composition of the spark-cut surface varies but that it is always Zn depleted.

polished surface [Fig. 4(a)]. The latter was exposed by cleaving a sample such that the cleave plane was perpendicular to a spark-cut surface; the cleaved surface was then polished to ensure that it was flat and perpendicular to the incident electron beam. We estimate that the spatial resolution of the EDX probe is $\sim 1\,\mu$m in all directions[14].

The EDX spectra taken on nominally $ZrZn_2$ surfaces [see Fig. 4(c)] contain three characteristic X-ray emission peaks that provide useful information about sample composition: Zn-Lα (1.0 keV), Zr-Lα (2.0 keV) and Zn-Kα (8.6 keV). The spectra in Fig. 4 show at a glance that the Zr peak is enhanced relative to both Zn peaks on the spark-cut surface compared to the polished surface, suggesting that spark erosion causes Zn depletion at the surface. We verified this by quantitative EDX analysis using spectra obtained both on $ZrZn_2$ samples and on pure element standards in identical conditions; for each peak i, the ratio k_i of peak area in the $ZrZn_2$ spectrum to that in the spectrum of the pure element standard was found. To a first approximation, the mass concentration of each element in the test sample is given by these standard-normalized peak areas k_i. However, it is well known that corrections[14] must be applied to take account of the way in which the composition of the test sample affects e.g. the electron beam penetration and the absorption of generated X-rays. Therefore we used a standard iterative ZAF (atomic number, absorption and fluorescence) correction procedure as implemented in the CITZAF package[15] to give accurate atomic concentrations, which are summarized in Table I. The quantitative result for the polished surface is in good agreement with the nominal atomic concentration (i.e. 33.3% Zr, 66.7% Zn) and the small difference is within the error arising from imperfect ZAF correction as discussed later. There is no dependence of the composition on distance from the spark-cut surface in the results shown for the polished surface, implying that any compositional change extends to a depth $\leq 1-2\,\mu$m. The results for the spark-cut surface show that the composition varies as a function of position but that it is always Zn-depleted, and that it includes regions that are close to Zr_2Zn in composition. Atomic concentrations shown in Table I are normalized to 100% but we note that no significant contaminant peaks are present in any of the spectra used to produce these results. For each sample spectrum two different composition estimates were obtained, the first using only the Zr-Lα and Zn-Kα peaks and the second using Zr-Lα and Zn-Lα. The presence of two characteristic Zn X-ray peaks of very different energy provides a check on our correction procedure because the correction factor is much larger for Zn-Lα than for Zn-Kα. The excellent agreement between the two estimates for the polished surface shows that the correction procedure pro-

vides accurate results in this ideal geometry. The small discrepancy (at the 1% atomic concentration level) may arise, for example, from the correction model used or from a slight tilt of the sample surface relative to the electron beam. Importantly, the results for the spark-cut surface obtained using the different Zn peaks are also in good agreement. The discrepancy is larger than in the case of the polished surface due to the effects of surface roughness on the X-ray intensity corrections. However, it is still small compared to the dramatic Zn depletion observed. Thus, we have shown that cutting $ZrZn_2$ by spark erosion causes the formation of a Zn-depleted surface layer of thickness $\leq 1 - 2\,\mu$m.

IV. DISCUSSION

We have demonstrated that $ZrZn_2$ is very susceptible to surface damage caused by spark erosion. The spark erosion process causes the surface layer to be depleted of Zn. Removal of the remaining Zr-rich surface layer requires an HF-based etch or electropolishing. In the course of this work we have found that un-etched spark-cut regions can easily be left on the surface if they are protected, for example, by organic material such as remnants of Ag/epoxy paint contacts. The resulting samples show resistive downturns like those observed in Ref. 9. Although the resistivity measurements reported in Ref. 9 were made with contacts on cleaved surfaces, the current path included remnants of spark-cut surfaces.

Our EDX measurements show that although the composition of the spark-cut surface varies in space, it is always more Zr-rich than $ZrZn_2$. The high mobility of Zn in the surface layer of $ZrZn_2$ is likely to be connected with the low melting point of Zn, $T_m = 419.6$°C. No regions of elemental Zr or Zn were observed at the $1\,\mu$m resolution of the EDX probe. Thus the simplest explanation for our results is that the observed downturns in $\rho(T)$ and $\chi(T)$ are due to a surface layer of a superconducting alloy, with higher Zr content than $ZrZn_2$, that is created by spark erosion. It is unlikely that spark cutting produces pure Zr because of the high solubility of Zn in Zr [10,11]. Other scenarios are also possible. One intriguing possibility is that spark erosion creates strained layers near the surface which are superconducting[16].

A feature of the spark-erosion-induced superconducting layer in $ZrZn_2$ is its large critical field to critical temperature ratio. It is well known that the critical field of a superconducting sample is enhanced with respect to the bulk thermodynamic critical field B_c when the sample is sufficiently small in at least one direction $\perp \mathbf{B}$ to allow penetration of magnetic flux[17]. For example, Al films of thickness 250 Å can show $T_{\rm SC} \approx 1.7\,$K and a critical field of 1.9 T [18]. Fig. 1(f) demonstrates this effect in a film of Zr: the critical field of the film is $\sim 1\,$T (close to the paramagnetic limit $B_c^{\rm para} = 1.84\,T_c$ [19,20]) compared to that of bulk Zr, $B_c \approx 0.0047$ T [21]. A similar enhancement is likely to occur in spark-eroded $ZrZn_2$ at any regions of the superconducting layer that are thin compared to the penetration depth.

We now comment on the pressure dependence of $T_{\rm SC}$ and $T_{\rm FM}$. Ref. 9 suggested that superconductivity and ferromagnetism vanished simultaneously at a critical pressure $p_c \sim 20\,$kbar. More detailed measurements of $T_{\rm FM}(p)$ [22] have now shown that ferromagnetism in fact disappears in a first order transition at a lower pressure $p_c({\rm FM}) = 16.5\,$kbar. Unfortunately no new data are available for $T_{\rm SC}(p)$, but the results in Ref. 9 show that $13 < p_c({\rm SC}) < 22\,$kbar. Thus the two p_c's lie close to each other, but further measurements of $T_{\rm SC}(p)$ would be needed to establish whether the superconductivity of the surface layer is related to ferromagnetism in the bulk.

V. CONCLUSIONS

In summary, spark erosion induces a superconducting layer in $ZrZn_2$. If this surface layer is removed by chemical etching the resistive superconducting transition disappears. EDX analysis of spark-cut surfaces shows that they are Zn depleted. The simplest explanation for the induced superconductivity is that it is due to a change in chemical composition caused be the spark erosion. It remains to be seen whether higher quality $ZrZn_2$ is superconducting at ambient pressure and above.

VI. ACKNOWLEDGEMENTS

We are grateful to A. Carrington and G. G. Lonzarich for useful discussions.

* Present address: Physik-Department E21, Technische Universität München, D-85747 Garching, Germany

[1] B. T. Matthias and R. M. Bozorth, Phys. Rev. **109**, 604 (1958).
[2] A. J. Leggett, J. Phys. (Paris), Colloq. **39**, C6-1264 (1978).
[3] D. Fay and J. Appel, Phys. Rev. B **22**, 3173 (1980).
[4] T. F. Smith, J. A. Mydosh, and E. P. Wohlfarth, Phys. Rev. Lett. **27**, 1732 (1971).
[5] R. L. Falge and R. A. Hein, Phys. Rev. **148**, 940 (1966).
[6] M. K. Wu, C. W. Chu, J. L. Smith, A. L. Giorgi, C. Y. Huang, B. T. Matthias, and F. E. Wang, Sol. Stat. Comm. **34**, 507 (1980).
[7] H. G. Cordes, K. Fischer, and F. Pobell, Physica B **107**, 531 (1981).
[8] S. Z. Huang, M. K. Wu, R. L. Meng, and C. W. C. amd J. L. Smith, Sol. Stat. Comm. **38**, 1151 (1981).
[9] C. Pfleiderer, C. M. Uhlarz, S. M. Hayden, R. Vollmer, H. von Löhneysen, N. R. Bernhoeft, and G. G. Lonzarich,

Nature (London) **412**, 58 (2001).
[10] R. P. Elliott, *Constitution of Binary Alloys, First Supplement* (McGraw-Hill, 1965).
[11] T. B. Massalski, J. L. Murray, L. H. Bennett, and H. Baker, *Binary Alloy Phase Diagrams* (American Society for Metals, Metals Park, OH, 1986).
[12] L. W. M. Schreurs, H. M. Weijers, A. P. J. V. Deursen, and A. R. Devroomen, Mat. Res. Bull. **24**, 1141 (1989).
[13] S. J. C. Yates, G. Santi, S. M. Hayden, P. J. Meeson, and S. B. Dugdale, Phys. Rev. Lett. **90**, 057003 (2003).
[14] V. D. Scott, G. Love, and S. J. B. Reed, *Quantitative Electron-Probe Microanalysis* (Ellis Horwood, New York, London, 1995).
[15] J. T. Armstrong, Microbeam Analysis **4**, 177 (1995).
[16] N. Kimura, M. Endo, T. Isshiki, S. Minagawa, A. Ochiai, H. Aoki, T. Terashima, S. Uji, T. Matsumoto, and G. G. Lonzarich, Phys. Rev. Lett. **92**, 197002 (2004).
[17] M. Tinkham, *Introduction to Superconductivity* (McGraw-Hill, 1975).
[18] M. Strongin and O. F. Kammerer, Phys. Rev. Lett. **16**, 456460 (1966).
[19] A. M. Clogston, Phys. Rev. Lett. **9**, 266 (1962).
[20] B. S. Chandrasekhar, Appl. Phys. Lett. **1**, 7 (1962).
[21] D. R. Lide, ed., *CRC Handbook of Chemistry and Physics 85th Edition* (CRC Press, Boca Raton, FL, 2004).
[22] M. Uhlarz, C. Pfleiderer, and S. M. Hayden, Phys. Rev. Lett. **93**, 256404 (2004).